Accuracy Assessment of CT-Based 3D Bone Surface Reconstruction

L. Puggelli[1], F. Uccheddu[1], Y. Volpe[1], R. Furferi[1(✉)], and D. Di Feo[2]

[1] Department of Industrial Engineering, University of Florence, Via di Santa Marta 3, 50139 Florence, Italy
rocco.furferi@unifi.it

[2] Department of Pediatric Surgery, A. Meyer Children's University Hospital, Viale Pieraccini 24, 50139 Florence, Italy

Abstract. 3D reconstruction of human anatomy from cross-sectional imaging has recently gained increasing importance in several medical fields thus designating the 3D bones reconstruction accuracy, critical for the success of the whole surgical intervention. The 3D anatomic model quality depends on the quality of the reconstructed image, on the quality of the images segmentation step and on the error introduced by the iso-surface triangulation algorithm. The influence of image processing procedures and relative parametrization has been largely studied in the scientific literature; however, the analysis of the direct impact of the quality of the reconstructed medical images is still lacking. In this paper, a comparative study on the influence of both image reconstruction algorithm (standard and iterative) and applied kernel is reported. Research was performed on the 3D reconstruction of a pig tibia, by using Philips Brilliance 64 CT scanner. At the stage of scanning and at the stage of 3D reconstruction, the same procedures were followed, while only image reconstruction algorithm and kernel were changed. The influence of such selection on the accuracy of bone geometry was assessed by comparing it against the 3D model obtained with a professional 3D scanner. Results show an average error in reconstructing the geometry of around 0.1 mm with a variance of 0.08 mm. The presented study highlights new opportunities to control the deviations on the geometry accuracy of the bones structures at the stage of cross sectional imaging generation.

Keywords: 3D model reconstruction · Kernel reconstruction · Accuracy · Computed tomography

1 Introduction

In many surgical fields (e.g. personalized cranio-maxillofacial surgery) computer-aided bone surgery requires highly accurate 3D representation of patient's bone, both for surgery planning and for implant design [1, 2].

The overall quality of a 3D anatomic model reconstruction, strictly depends on (i) the quality of the patient CT scan data, (ii) on the quality of the images processing step and (iii) on the errors introduced by the iso-surface triangulation algorithm (i.e. extract a 2D surface mesh from a 3D volume). The medical imaging quality mainly affects the spatial resolution depending on the type of computer tomography

F. Cavas-Martínez et al. (Eds.): *Advances on Mechanics, Design Engineering and Manufacturing II*, LNME, pp. 487–496, 2019.
https://doi.org/10.1007/978-3-030-12346-8_47

(CT) system and on the chosen scanning parameters. The spatial resolution depends also by the size of the voxel influenced by the slice thickness and by the matrix size. Changing the slice thickness can create a partial volume effect that needs to be considered for segmentation, and final 3D surface reconstruction [3–8]. The research community is working toward the determination of the relation between 3D model accuracy and image processing [9–13], including image enhancement and segmentation. Currently, a challenging task remains the determination of the relation between accuracy of the resulting 3D model and the medical data generation.

The quality of the resulting 3D anatomic model is, however, highly related to the quality of the reconstructed images, generally performed on board of the Computer Tomography scanner; the reconstruction chain, relies on a number of algorithms specifically designed to simultaneously optimize the imaging speed, the dose efficiency, and the general image quality. CT scans allows a number of reconstruction algorithms and relative kernels; the most appropriate combination depends on which tissues should be more or less highlighted. The Filtered back projection (FBP) method, due to its velocity and robustness, is the most common method used on-board of the clinical available CT scanners to reconstruct the cross-sectional images from raw data. However, FBP proved to be a sub-optimal algorithm choice for poorly sampled data or for cases where noise has a significant power density compared to the measured signal.

When these very high levels of noise are propagated through the reconstruction algorithm, the result is an image with significant artefacts. Way et al. [14] show that the fine tuning of the FBP parameters (i.e. the most important parameter is the reconstruction kernel), can significantly improve the quality of the resulting reconstructed images. In real clinical settings, once the images are reconstructed, the projection data is removed from the system, making further reconstruction with a different reconstruction filter parameter set impossible. Okubo et al. [15] proposed a method based on common image filtering techniques in the image space to be used instead of a reconstruction filter in the projection space for CT imaging, to achieve similar image quality.

The goal of this study is to assess the 3D accuracy of CT-based bone surface reconstruction, at varying the CT scanner internal parameters. More in detail, this study investigates into the influence of kernel selection in the image reconstruction algorithm about the accuracy of the 3D reconstruction, independently from the segmentation thresholding and from the surface reconstruction algorithms.

The study was performed in the Meyer Children's Hospital premises on a pork shank with and without soft tissues. This allows direct comparison between the CT-based reconstructions, obtained using different kernels, and the 3D model of the shank bone obtained using a professional 3D scanner.

2 From CT Scan Data to 3D Polygonal Model

According to recent literature [3], the most effective way for creating 3D models starts from the image processing of the medical image acquisition, by enhancing and segmenting some region of interest, then, converting the result into 3D models, through surface reconstruction procedures. The main steps of the pipeline are described in the following sections.

2.1 Medical Imaging Data Generation

The scan of the patient body is clinically performed by first appropriately tuning some machine parameters, which influences the final CT images.

X-rays tube potential [kV] and *current* [mAs] determine the energy of the ionizing radiation; therefore, they influence the patient adsorbed dose, i.e. the mean energy imparted to mass per unit mass by ionizing radiation. On the other hand, higher energy corresponds to more saturated images.

Scan range [mm] is the actual axial dimension of the section to be scanned. It is set to cover only the body region to investigate.

Pitch [mm/s] is the axial translation per rotation or the axial speed/the ratio between axial speed and collimation thickness.

Rotation time [s] is the time that the X-ray generators/detectors require to complete a single rotation around the axis.

Acquisition thickness [mm] is the virtual spacing between the acquired slices. A higher number of slices improve the detail in the scanning axis; on the other hand, both the time needed to complete the scan and the time to reconstruct the images increase.

These parameters directly act on the raw acquisition phase, while the *reconstruction algorithm* selection and the *reconstructed slice thickness* parameter, act on the medical image reconstruction phase. The raw data at the end of the CT acquisition is a sinogram [16] i.e. the Radon Transform of acquired data. Figuring the sinogram as an image, each one of its rows corresponds to the acquired data for each axial position, and each pixel of a selected row corresponds to the acquired datum for that axial position at a known angular position.

The *reconstructed slice thickness* [mm] is the spacing between the reconstructed slices, since it can be calculated interpolating the raw data, it does not necessarily coincides with the *acquisition thickness*: its value is usually equal or less.

Raw data must be elaborated in order to obtain the corresponding series of slices, by means of *Image reconstruction algorithms* based on Radon anti-transform e.g. the Filtered back projection (FBP) method, is commonly used on-board of the clinical available CT scanners to reconstruct the cross-sectional images from raw data [16]. Depending on the specific CT scan device, (ASIR™—GE, iDose^{4}®—Philips NV, IRIS®—Siemens AG, AIDR®—Toshiba Corporation, to cite some), a number of proprietary algorithms are available [17–19]. The fine-tuning of the FBP parameters (e.g. reconstruction kernels), can significantly improve the quality of the resulting reconstructed images when data are poorly sampled, or when the noise has a significant power density compared to the measured signal. Different kernels can be used optimally for different tissues, thus allowing highlighting some anatomical feature in the region of interest.

The reconstruction kernels may operate into the image domain or into the sinogram domain. Essentially, kernels are applied in order to enhance contrast resolution (low-pass or smoothing filters) or to enhance spatial resolution (high-pass or edge enhancement kernels). Each CT scan producer adopt different names for these kernels, e.g. *Detail*, *Bone* or *Edge* for edge enhancement kernels and *Standard* or *Soft* for smoothing kernels.

2.2 Image Processing and Surface Modelling

In order to further improve the classification of the different tissues on the CT scan images (i.e. bones, soft tissue or tumours), several image processing tools can be applied offline to the 2D dataset. A first image enhancement can be performed to suppress artefacts or to highlight the tissues borders. Then, a *segmentation* step is needed to identify the tissues boundaries. Segmentation is the process of dividing an image into regions with similar properties [20]. The role of segmentation on medical imaging, consists in identifying the anatomical structures in the images. As result of the segmentation task, the pixels in the image are partitioned through binary masks, in non-overlapping regions, belonging to the same tissue class. When the region of interested is naturally highlighted, as for the case of bone structures that shows high grey level pixels, an automatic thresholding can be performed to separate the bone pixels from the rest of the image.

After the segmentation phase, starting from the obtained multi slices binary masks (i.e. voxels), the 3D surface are generated by applying *Marching cubes* algorithms or other 3D contour extraction algorithms [21]. All the functions that are required to obtain a 3D polygonal model from a series of slices are included in many dedicated software, like *Mimics*® and *3D Slicer*® (Fig. 1).

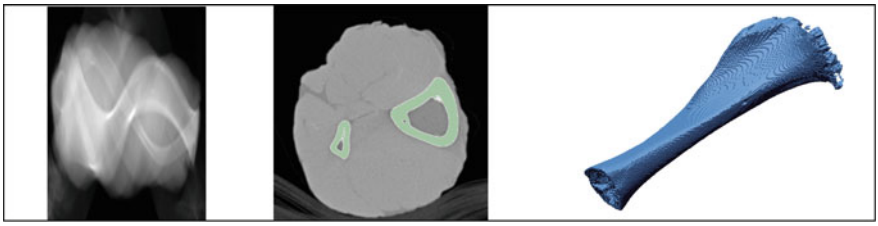

Fig. 1. From sinogram to polygonal model

3 Experimental Design

3.1 CT Scanning and Medical Images Reconstruction

CT scanning has been performed on a *Brilliance 64 CT* spiral scanner (*Philips NV*, Eindhoven, Netherland). Machine parameters (see Table 1), and in particular tube potential and tube current, have been set at standard values for children (i.e. 100 kV and 200 mAs respectively). In order to obtain a small spacing between reconstructed slices, acquisition spacing has been set at 0.8 mm. Scan range, which depends on the size of the subject to be scanned, has been adjusted at 170 mm as the size of the pig tibia.

From a single scan (i.e. from a single sinogram), six different series of images have been reconstructed by adopting both Philips image reconstruction algorithms (*Standard* and *iDose4*®) and by applying three different kernels respectively: *Smooth* (low pass filter), *Sharp* and *Bone* (high pass filters). The nomenclature adopted for the series

Table 1. CT-scan settings

Parameters	Value
Tube potential	100 kV
Tube current	200 mAs
Scan range	170 mm
Acquisition thickness	0.8 mm

makes use of the kernels DICOM acronym (A = *Smooth*, C = *Sharp*, D = *Bone*), while "S" and "I" indicates *Standard* or *iDose4*® image reconstruction algorithm [20].

3.2 3D Reconstruction from CT-images

From reconstructed medical images, the entire procedure of 3D reconstruction have been implemented by means of *3D Slicer*® software, one of the most popular free and open source software package for medical image computing and visualization [22]. In order to limit the influence of the image-processing phase, no enhancement filters have been applied to the images, and the segmentation of the bones have been performed through a thresholding operation. In this phase, a threshold value of 700 Hounsfield Unit (HU) has been used: this value corresponds to the linear attenuation coefficient associated to cortical bones [17]. As a consequence, only the diaphysis of the tibia has been opportunely reconstructed, while epiphysis and metaphysis—which have $250 \cdot \mathrm{HU} \cdot 700$ typical values (due to high concentration of cancellous bone)—have not been correctly detected.

Finally, the 3D polygonal model of each segment has been retrieved by means of the *Marching cubes* algorithm implemented into *3D Slicer*®, in which smoothing factor has been maintained at 0. Each reconstructed 3D polygonal model has been exported in the form of STL file. For a sake of clarity, the same nomenclature as slides series has been maintained (e.g. R_SA→R_SA.stl).

3.3 3D Laser Scanning

To obtain a high-accurate 3D virtual reconstruction of the tibia to be used as ground-truth, the dry bone (i.e. after soft tissues removal by boiling) has been acquired by means of a 3D laser scanner (*Romer Absolute Arm RA 7520 SI* with integrated *RS1* laser scanner). Such a scanner provides a volumetric accuracy in the range ± 0.058 mm within the measurement range of 2.0 m and a point repeatability lower than 0.023 mm, according to the ASME B89.4.22 certification. Both acquisition and successive 3D reconstruction operations have performed by means of *Polyworks*® software.

As soft tissues are present in the acquired CT-data, and as boiling of the pig bone may have an impact on its geometry and, consequently, on the successive accuracy assessment phase, steps 1–3 have been repeated on the dry tibia (i.e. without soft tissues), maintaining the same procedures and parameters. For this reason, 6 additional polygonal models have been used (B_XX series).

3.4 Comparison & Accuracy Assessment

CT-based reconstructions and ground truth have been imported as STL files into *Geomagic Design X*® software environment. Before performing accuracy measurements, two main operations have been carried out:

1. Invalid portions removal from each STL mesh;
2. Alignment between scan data.

As previously partially reported, CT-based polygonal models present an incomplete reconstruction of cancellous bone sections of tibia (i.e. epiphysis and metaphysis) due to segmentation at 700 HU. In addition, such models also include internal cavities of the bone, which have not been measured by means of laser scanner. In order to avoid imprecise alignment and invalid accuracy assessment, all of these portions on each mesh have been ignored.

Successively, all the polygonal models have been aligned referring to R_XX models (which are natively aligned since deriving from the same CT-scanning). To come up with this purpose, both *point-to-point* and *ICP* algorithms have been used [23].

At this point, accuracy of each CT-based STL has been assessed by comparing it against ground-truth. This operation has been carried out by means of *mesh max deviation* tool, which computes the distance between each point on a *target* and its projection on a *reference* mesh (i.e. ground-truth), along the target mesh normal. Then, for each element of the target, the maximum distance is considered.

4 Results and Analysis

Following the procedure described in Chap. 3, in Table 2 both mean (μ) and standard deviation (σ) resulting from the analysed mesh deviations are reported (see Fig. 2).

Table 2. Mesh deviation analyses

3D models	Signed dist. [mm]		Unsigned dist. [mm]		Mesh%	
	μ	σ	μ	σ	$\lvert d\rvert < 0.1$ mm	$\lvert d\rvert < 0.2$ mm
R_SA	0.141	0.128	0.162	0.101	31.7	64.2
R_SC	0.113	0.114	0.134	0.089	40.3	76.5
R_SD	0.113	0.115	0.134	0.089	40.4	76.7
R_IA	0.142	0.127	0.162	0.100	31.6	64.2
R_IC	0.113	0.114	0.134	0.089	40.3	76.5
R_ID	0.113	0.115	0.134	0.115	40.4	76.7
B_SA	–0.134	0.145	0.160	0.115	35.7	65.8
B_SC	–0.039	0.137	0.115	0.083	49.5	83.0
B_SD	–0.029	0.137	0.114	0.082	50.1	83.7
B_IA	–0.134	0.145	0.160	0.115	35.7	65.8
B_IC	–0.039	0.137	0.115	0.083	49.5	83.0
B_ID	–0.029	0.137	0.114	0.082	50.1	82.4

In all the analyzed comparisons, only little differences are visible: μ is between ± 0.13 mm (signed distance) or between 0.11 ÷ 0.16 mm (unsigned distance) and relative σ is between 0.11 ÷ 0.14 mm (signed distance) or between 0.08 ÷ 0.11 mm (unsigned distance).

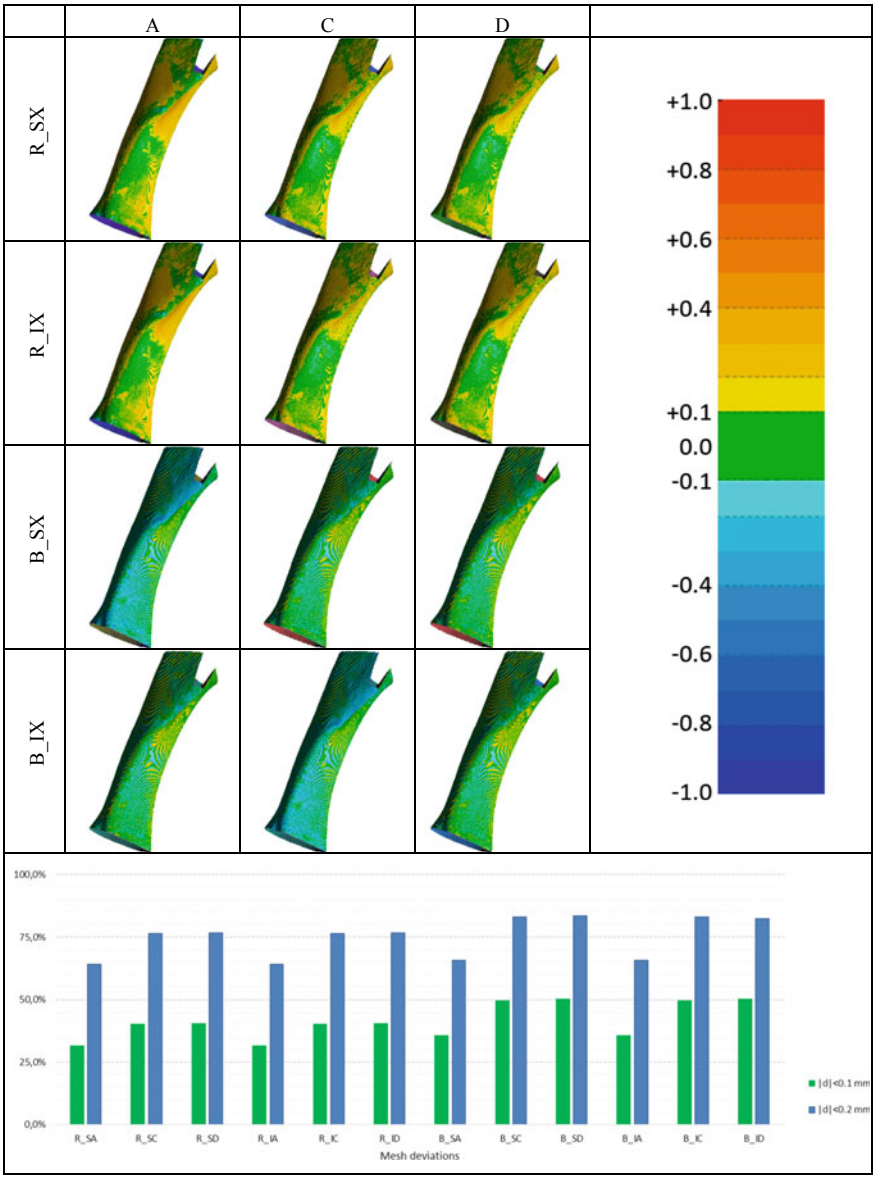

Fig. 2. Obtained mesh deviation maps

In addition, 3D reconstructions obtained by means of *Standard* and *iDose*$^{4®}$ algorithms show almost the same identical statistical values, even if slide images visibly differ. This lead to suppose that *iDose*$^{4®}$ helps in augmenting the readability of medical images without affecting bones silhouette and, on the other hand, that there is no evident reason to adopt *iDose*$^{4®}$ to 3D reconstruction purposes, since it is more time consuming with respect to *Standard* algorithm. The same observation is still valid for what concerns the kernel choice. However, in this case, some slightly differences are numerically visible between *Smooth* (*A*) kernel and both *Sharp* (*C*) and *Bone* (*D*) kernels.

Especially paying attention to the two last columns of Table 2, it emerges that in the analysed case study, the mesh percentage of R_XA beneath $|d| < 0.1$ is almost 30% lower than R_XC or R_XD, while no tangible difference appears between the latter two (31.7 vs. 40.3% and 40.4%). Similar values are reported when analysing the mesh percentage of R_XA beneath $|d| < 0.2$ (20% lower, 64.2 vs. 76.5% and 76.7%). Similar consideration are valid also for all B_XX polygonal models.

On the light of this analysis on this case study, even if difference is almost invisible and probably negligible, it seems to be suggestable the adoption of *Standard* image reconstruction algorithm with *Sharp* or *Bone* kernel.

5 Conclusion and Future Developments

In this paper, authors report a first investigation into the influence of kernel choice in the accuracy of a CT-based 3D reconstructed polygonal model. In particular, attention has been focused on *Brilliance 64 CT* spiral scanner (*Philips NV*, Eindhoven, Netherland) and relative image reconstruction algorithms (*Standard* and *iDose*$^{4®}$). The reconstruction of a pig tibia has been used as case study. Three different kernels have been selected a priori due to their relevance: *Smooth, Sharp* and *Bone*. Tube voltage, tube current and *iDose*$^{4®}$ level have been maintained constant and the same procedure to reconstruct 3D polygonal model from CT-images has been followed. Accuracy of each CT-based 3D reconstruction has been assessed by comparing the resulting polygonal model against a high-accurate 3D virtual model, considered as ground-truth, obtained by means of Romer Absolute Arm and RS1 3D laser probe. Mesh deviation analyses showed no evident difference varying image reconstruction algorithm and kernel. However, two main observations have to be made: 1. there is an almost total overlap between 3D reconstructions obtained with *Standard* and *iDose*$^{4®}$, making the first preferable due to less computational time; 2. *Sharp* and *Bone* kernels provide slightly more accurate 3D reconstruction with respect to *Smooth* one. Despite limited to a single case study, this analysis paves the way for a correct use of different kernels in TC scanning, thus allowing the choice of the best option when the main intent is to reconstruct the 3D anatomy of bones.

References

1. Fuessinger MA et al (2018) Planning of skull reconstruction based on statistical shape model combined with geometric morphometrics. Int J Comput Assist Radiol Surg 13(4):519–529
2. Marreiros FMM et al (2016) Custom implant design for large cranial defects. Int J Comput Assist Radiol Surg 11(12):2217–2230
3. Rengier F et al (2010) 3D printing based on imaging data: review of medical applications. Int J Comput Assist Radiol Surg 5(4):335–341
4. Lee Ventola C (2014) Medical applications for 3D printing: current and projected uses. P and T 39(10):704–711
5. Do A-V et al (2015) 3D printing of scaffolds for tissue regeneration applications. Adv Healthc Mater 4(12):1742–1762
6. Choi JW, Kim N (2015) Clinical application of three-dimensional printing technology in craniofacial plastic surgery. Arch Plast Surg 42(3):267–277
7. Ridwan-Pramana A et al (2016) Structural and mechanical implications of PMMA implant shape and interface geometry in cranioplasty—a finite element study. J Cranio-Maxillofac Surg 44(1):34–44
8. Park E-K et al (2016) Cranioplasty enhanced by three-dimensional printing: custom-made three-dimensional-printed titanium implants for skull defects. J Craniofac Surg 27(4): 943–949
9. Stull KE et al (2014) Accuracy and reliability of measurements obtained from computed tomography 3D volume rendered images. Forensic Sci Int 238:133–140
10. Lalone EA et al (2015) Accuracy assessment of 3D bone reconstructions using CT: an intro comparison. Med Eng Phys 37(8):729–738
11. Gelaude F, Vander Sloten J, Lauwers B (2008) Accuracy assessment of CT-based outer surface femur meshes. Comput Aided Surg 13(4):188–199
12. Tan CJ et al (2017) Influence of scan resolution, thresholding, and reconstruction algorithm on computed tomography-based kinematic measurements. J Biomech Eng 139(10):104503
13. Naddeo F et al (2017) An automatic and patient-specific algorithm to design the optimal insertion direction of pedicle screws for spine surgery templates. Med Biol Eng Comput 55(9):1549–1562
14. Way TW et al (2008) Effect of CT scanning parameters on volumetric measurements of pulmonary nodules by 3D active contour segmentation: a phantom study. Phys Med Biol 53(5):1295–1312
15. Ohkubo M et al (2011) Image filtering as an alternative to the application of a different reconstruction kernel in CT imaging: feasibility study in lung cancer screening. Med Phys 38 (7):3915–3923
16. Brooks RA, Chiro DG (1976) Principles of computer assisted tomography (CAT) in radiographic and radioisotopic imaging. Phys Med Biol 21(5):689–732
17. Li H et al (2016) A comparative study based on image quality and clinical task performance for CT reconstruction algorithms in radiotherapy. J Appl Clin Med Phys 17(4):377–390
18. Beister M, Kolditz D, Kalender WA (2012) Iterative reconstruction methods in X-ray CT. Physica Med 28(2):94–108
19. iDose^4 Technical White-paper: http://incenter.medical.philips.com/doclib/enc/fetch/2000/4504/577242/577249/586938/587315/iDose4_-_Whitepaper_-_Technical_-Low_Res.pdf%3fnodeid%3d8432599%26vernum%3d-2
20. Uccheddu F et al (2017) 3D printing of cardiac structures from medical images: an overview of methods and interactive tools. Inter J Interact Des Manuf (Article in press)

21. Lorensen WE, Cline HE (1987) Marching Cubes: a high resolution 3D surface construction algorithm. Comput Graph (ACM) 21(4):163–169
22. Fedorov A et al (2012) 3D Slicer as an image computing platform for the quantitative imaging network. Magn Reson Imaging 30(9):1323–1341
23. Besl PJ, McKay ND (1992) A method for registration of 3-D shapes. IEEE Trans Pattern Anal Mach Intell 14(2):239–256